Density Functional Theory Study of Magnetic Coupling in the $Gd_{12}O_{18}$ Cluster

Lixin Ning,*,†,§ Yongfan Zhang,‡ Zhifeng Cui,† Mario Italo Trioni,§ and Gian Paolo Brivio§

Department of Physics, Anhui Normal University, Wuhu, Anhui, 241000, People's Republic of China, Department of Chemistry, Fuzhou University, Fuzhou, Fujian, 350002, People's Republic of China, and Dipartimento di Scienza dei Materiali and CNISM, Università degli Studi di Milano-Bicocca, via Cozzi 53, 20125 Milano, Italy

Received: August 6, 2008; Revised Manuscript Received: September 20, 2008

The magnetic properties of the $Gd_{12}O_{18}$ cluster cut from the bulk Gd_2O_3 crystal are investigated using the spin-polarized density functional theory within the broken-symmetry approach. Our work reveals that in the ground state of the cluster the antiferromagnetic coupling between adjacent Gd ($4f^7$) spins is preferred energetically. This result is in contrast to a recent prediction made by Pedersen and Ojamäe (Pedersen, H.; Ojamäe, L. *Nano Lett.* 2006, *6*, 2004) but is consistent with recent experimental observations. The optimized structures of the cluster in the lowest-energy broken-symmetry state and the highest-spin ferromagnetic state are almost identical. The latter state is 71.5 cm^{-1} higher in energy than the former one, giving a value of about -0.24 cm^{-1} for the magnetic coupling constant, which is comparable to that estimated from experiments on the bulk crystal. The relative energies of various $4f^7$ spin patterns of the cluster are calculated, and certain characteristics of the cluster in the lowest-energy broken-symmetry state are discussed.

I. Introduction

Lanthanide-doped nanomaterials have attracted considerable attentions due to their wide variety of potential applications in areas such as solid-state lasers, lighting and displays, and fluorescence labeling.[1,2] Among these materials, Gd_2O_3 nanoparticles are of particular interest. Besides the good chemical durability, thermal stability, low phonon energy, and easiness of doping with other lanthanide ions,[3−5] these particles have the additional advantage that they may function as contrast agents for medical magnetic resonance imaging (MRI) as Gd^{3+} is a known MRI agent.[6−8] Recently it was reported that Gd_2O_3 nanoparticles demonstrated a positive contrast effect for T_1-weighted imaging and displayed the potential applications as MRI agents at the same time as fluorescence labels to achieve multi-imaging in vivo.[9−11] To understand the physical properties of Gd_2O_3 nanoparticles, which are required for their applications, it is very necessary to relate the properties to their geometric and electronic structures using modern computational techniques. Pedersen and Ojamäe[12] have made such an attempt to understand their magnetic properties by employing a model $Gd_{12}O_{18}$ cluster constructed from the bulk crystal. Using density functional theory (DFT), they calculated the total energies of the cluster in states with different spin multiplicities at the B3LYP/6-31G level of theory and obtained a ferromagnetic high-spin ($S = 84/2$) ground state in which all Gd ($4f^7$) spins are aligned parallel. The calculation suggests that the cluster could exhibit superparamagnetic behavior similar to that observed with iron oxide nanoparticles.[13] This is surprising in view of the fact that in the ground state of the bulk Gd_2O_3 crystal, the magnetic coupling between nearest-neighbor Gd ions was experimentally found to be antiferromagnetic.[14] Moreover, recent experiments on the magnetic properties of ultrasmall Gd_2O_3 nanoparticles also showed that the particles exhibit paramagnetic rather than superparamagnetic behavior.[10]

We note that surface interactions may be important for magnetism of nanoparticles where a large fraction of ions are at the surface with their coordination number smaller than that of ions within the bulk crystal. For example, in the case of small nanoparticles made of ferromagnetic materials such as iron, nickel, and cobalt, the surface magnetic moments are enhanced by 10−30% over their bulk values.[15] However, in the case of $Gd_{12}O_{18}$ considered here, although all the Gd^{3+} ions are located at the surface, the magnetic coupling would not be expected to change significantly with respect to that in the bulk crystal. This is because the spin-only magnetic moment of Gd^{3+} is highly localized in the half-filled 4f shell. These features can be observed even in the bulk hexagonal close-packed Gd metal.[16]

Quantitative descriptions of magnetic coupling have been a challenging task and require state-of-the-art computational efforts on the basis of either wave function-based or DFT-based methods. Illas and co-workers have recently reviewed the conceptual and theoretical issues concerning these quantitative methods.[17,18] In the present work, we carry out an investigation for the magnetic coupling in the $Gd_{12}O_{18}$ cluster aiming at understanding the magnetic behavior of small Gd_2O_3 nanoparticles. For this purpose, we calculated the relative total energies of $Gd_{12}O_{18}$ in states with different spin multiplicities, using the spin-polarized DFT (SDFT) method within the broken-symmetry approach. Our study shows that the ground state of $Gd_{12}O_{18}$ is in fact an antiferromagnetic (AFM) state rather than a ferromagnetic (FM) one, and the cluster should exhibit a paramagnetic behavior. The computational methods and details are described in section II, and the results of the calculations are presented and discussed in section III. The final conclusions are collected in section IV.

II. Computational Methods

II.A. Broken-Symmetry Approach. The present investigation involves a computational determination of magnetic

* Corresponding author. E-mail: ninglx@mail.ahnu.edu.cn.
† Anhui Normal University.
‡ Fuzhou University.
§ Università degli Studi di Milano-Bicocca.

10.1021/jp807015b CCC: $40.75 © 2008 American Chemical Society
Published on Web 12/02/2008

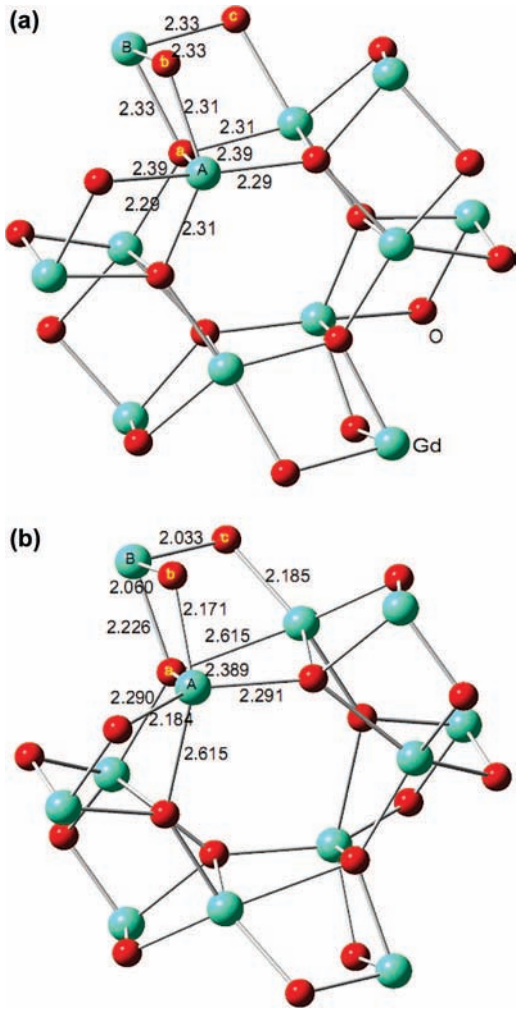

Figure 1. Structures of the $Gd_{12}O_{18}$ cluster obtained from the bulk crystal (a) and from geometry optimization (b), viewed along the S_6 symmetry axis. Selected Gd−O bond lengths are given in angstroms.

coupling between Gd^{3+} ions in the $Gd_{12}O_{18}$ cluster. The exchange interaction between these ions may be phenomenologically described by the Heisenberg−Dirac−Van Vleck (HDVV) spin Hamiltonian:[19−21]

$$\hat{H} = -\sum_{i<j} J_{ij}\hat{S}_i \cdot \hat{S}_j \qquad (1)$$

where J_{ij} is the magnetic coupling constant describing the spin exchange between different spin states and $\hat{S}_i$ and $\hat{S}_j$ are the total spin operators for the Gd ions at the sites i and j, respectively. The sum extends over all pairwise exchange interactions between first-neighbor Gd ions which share two nearest-neighbor O atoms. There are a total of 18 such Gd pairs in the $Gd_{12}O_{18}$ cluster (see Figure 1a). The sign of the magnetic coupling constant is such that J_{ij} is positive (negative) for FM (AFM) coupling between ions i and j.

Before turning our attention to this polynuclear system, let us first consider the magnetic coupling between two Gd ions (at sites i and j) in proximity. The calculation of the magnetic coupling constant J_{ij} involves a computation of energies of high-spin and low-spin states. Because SDFT is generally implemented as a single-determinant method, pure spin eigenfunctions which are usually multiconfiguration wave functions are difficult to describe. The single-determinant description of the highest-spin state with $S = 7$ is not a problem, except for a small spin contamination inherent to the use of SDFT. For the low-spin states with $S = 0, 1,..., 6$, the eigenfunctions are expressed as linear combinations of Slater determinants and therefore are not amenable to direct SDFT calculations. Noodleman and co-workers[22−24] proposed an alternative approach in which a broken-symmetry single-determinant wave function is constructed and evaluated with the SDFT formalism, and its expectation value is used in combination with the spin projection method to estimate energies of pure spin states. This approach has been used to derive rules for interpreting and designing magnetic molecules and solids that incorporate transition metal ions and/or organic radicals.[17,18]

Recently, Hughbanks and co-workers have demonstrated the ability of the broken-symmetry approach to study magnetic properties of gadolinium-containing systems.[25−27] SDFT is first used to calculate the energy of $|\uparrow_7\uparrow_7\rangle$ and $|\uparrow_7\downarrow_7\rangle$, where $|\uparrow_7\uparrow_7\rangle$ represents a determinant where all seven of the 4f electrons on both Gd centers are spin up, and $|\uparrow_7\downarrow_7\rangle$ represents a determinant where all seven 4f electrons on one Gd center are spin up and all seven on the other are spin down. $|\uparrow_7\uparrow_7\rangle$ is an eigenfunction of the highest-spin state with $S = M_s = 7$, and $|\uparrow_7\downarrow_7\rangle$, which is the broken-symmetry state with $M_s = 0$, can be expressed as a linear combination of pure spin eigenfunction with $S = 0, 1,..., 7$, and $M_s = 0$. The SDFT energy of the $|\uparrow_7\uparrow_7\rangle$ state can be identified with the energy of the highest-spin state obtained with the HDVV Hamiltonian:

$$E_{|\uparrow_7,\uparrow_7\rangle} = \langle (S_iS_j)S|\hat{H}|(S_iS_j)S\rangle = -(1/2)J_{ij}[S(S+1) - 63/2] = -(49/4)J_{ij} \qquad (2)$$

where $S_i = S_j = 7/2$ and $S = 7$. For the broken-symmetry state, $|\uparrow_7\downarrow_7\rangle$, the SDFT energy is a weighted average of the pure spin state energies, with the weights being the squared Clebsch−Gordon coefficients, and can be solved to give $E_{|\uparrow_7\downarrow_7\rangle} = (49/4)J_{ij}$.[28] It is worth noting here that the energies of the $|\uparrow_7\uparrow_7\rangle$ and $|\uparrow_7\downarrow_7\rangle$ states obtained with the HDVV spin Hamiltonian could also be obtained with the Ising spin Hamiltonian, $\hat{H}_{\text{Ising}} = -J_{ij}\hat{S}_{iz} \cdot \hat{S}_{jz}$, which is generally used to describe the spin exchange interactions in magnetic solids. This point has been discussed at length in ref 28. The SDFT energy difference between the highest-spin and the broken-symmetry states can then be used to calculate the magnetic coupling constant from the equation

$$E_{|\uparrow_7,\downarrow_7\rangle} - E_{|\uparrow_7,\uparrow_7\rangle} = (49/2)J_{ij} \qquad (3)$$

from which the relative energies of the entire pure spin states can be derived. In order to qualitatively check whether a given system will exhibit AFM or FM coupling, it is useful to examine the characteristics of the broken-symmetry solution, although it does not actually represent any true wave function of the system. The structural and electronic factors that tend to (de)stabilize $|\uparrow_7\downarrow_7\rangle$ versus $|\uparrow_7\uparrow_7\rangle$will proportionally affect the (de)stabilization of the true wave function.

The idea presented above also applies to Gd pairwise interactions in the $Gd_{12}O_{18}$ cluster. Whereas there is only one broken-symmetry state in the dinuclear case, for this polynuclear system there is more than one. The lowest-energy broken-symmetry state is the one whose spin coupling pattern most resembles that in the spin ground state.[22−24] We shall discuss certain characteristics of the lowest-energy broken-symmetry state for the $Gd_{12}O_{18}$ cluster to gain insight into the origin of magnetic coupling in this polynuclear cluster.

II.B. Computational Details. The SDFT calculations have been carried out by using the hybrid B3LYP density functional[29,30] as implemented in the Gaussian03 program.[31] The hybrid functionals are the most accurate functionals available as far as

energetics is concerned[32] and are often the method of choice within computational lanthanide chemistry.[33−35] The present use of the B3LYP functional is also motivated by its ability to accurately predict the band gap energy for the bulk Y_2O_3 crystal.[36] The 6-31G(d) basis set was used for oxygen, whereas for gadolinium, the relativistic effective core potential (ECP) of CEP-31G coupled with the optimized [4s4p2d2f]-GTO valence basis set was employed.[37] This ECP treats [Kr]$4d^{10}$ as fixed cores, and only the $5s^25p^64f^75d^16s^2$ shell (18 electrons) is taken into account explicitly. The choice of the ECP and basis sets is based on a compromise between accuracy and practicability. No symmetry constraint was imposed during the geometry optimization. The optimized structures were confirmed by the frequency calculation at the same level to be the real minimum without any imaginary vibration frequency. The convergence criterion for energy was set at 10^{-8} au throughout the calculation.

III. Results and Discussion

III.A. Nuclear Geometries. The Gd_2O_3 lattice crystallizes in the cubic space group *Ia*3 (T_h^7, no. 206) and has 16 Gd_2O_3 formula per unit cell, with 24 of the Gd atoms at C_2 sites and the other eight at C_{3i} sites. The Gd atoms are each 6-fold coordinated, and the oxygen atom is 4-fold coordinated by one Gd atom in C_{3i} site and three Gd atoms in C_2 sites. The Gd−O bond lengths range from 2.29 to 2.39 Å. The positions of the lattice constituents can be found in ref 14. Following the procedure described in ref 12, the stoichiometric $Gd_{12}O_{18}$ cluster was cut from the bulk crystal with the (111) crystal plane as the dominant surface. The so-obtained cluster, as shown in Figure 1a, has an S_6 symmetry with no net dipole moment and contains two and three chemically nonequivalent Gd (indicated by A and B) and O (indicated by a, b, and c) atoms, respectively. Geometry optimizations have been performed for the broken-symmetry state with $M_s = 0$ and the highest-spin state with $M_s = 84/2$, the former being the lowest-energy broken-symmetry state (see below). The computed Gd−O distances are in the range of 2.184−2.615 Å and are slightly smaller in the lowest-energy broken-symmetry state than the corresponding ones in the highest-spin state, but they are the same up to the third digit; thus, only a single structure was plotted in Figure 1b. This result indicates that the 4f spin patterns in the cluster have negligible influence on its structure, an indication of the negligible participation of Gd 4f orbitals in bonding. After geometry optimization, the overall structure of the cluster remains unchanged, having an approximate S_6 symmetry. The size of the cluster is 0.94 nm as derived from the distance between the two most distant O atoms.

III.B. Magnetic Properties. The central results of our calculation are presented in Figure 2. Besides for the broken-symmetry state with $M_s = 0$ and the highest-spin state with $M_s = 84/2$, the spin patterns and relative total energies for the other broken-symmetry states with $M_s = 14/2, 28/2, 42/2, 56/2, 70/2$ are also presented, which were calculated using the optimized geometry of the $M_s = 0$ state. The number of the AFM-coupled Gd pairs in each spin pattern is also given. The results indicate clearly an energetic preference for the AFM coupling between adjacent Gd ($4f^7$) spins within the cluster. The energy of the highest-spin state is 71.5 cm^{-1} higher than that of the lowest-energy broken-symmetry state where a total of 12 pairs have their spins in opposite directions. From these and eq 3 we can estimate an average value for the magnetic coupling constant and obtain $J_{ij} \approx -0.35$ K (or -0.24 cm^{-1}). This value is comparable to that of about −0.27 K estimated for the bulk Gd_2O_3 crystal.[14] For convenience of later discussion, we will refer to the highest-spin and the lowest-energy broken-symmetry states as the FM and the AFM states, respectively.

Spin pattern	Relative total energy E (cm^{-1})	Number of AFM-coupled Gd pairs	M_s
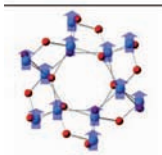	71.5	0	84/2
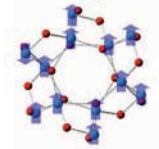	56.7	2	70/2
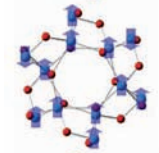	41.1	4	56/2
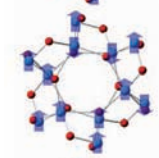	20.1	8	42/2
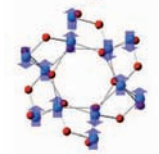	18.2	10	28/2
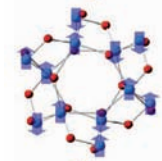	17.1	10	14/2
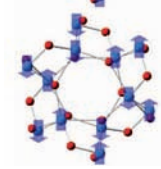	0.0	12	0

Figure 2. Spin patterns, relative total energies, and number of AFM-coupled Gd pairs for $Gd_{12}O_{18}$ in states with different multiplicities.

Population analyses are common ways to characterize the electronic structure of metal atoms. It was shown recently that the natural population analysis[38] is more suitable than the standard Mulliken population analysis for f-block metals.[35] A natural population analysis was thus carried out for the AFM and FM states of the $Gd_{12}O_{18}$ cluster. The resulting magnetic moments, electronic configurations, and natural charges on Gd and O atoms are presented in Table 1. One can see that for the AFM state, the magnetic moments on Gd atoms of type A are slightly smaller in magnitude than those of type B (by 0.03 μ_B), and their relative signs are shown schematically by the spin pattern in Figure 2. The induced magnetic moments on O atoms of type a are negligible, whereas for those of type b or c, two different magnitudes occur, the larger (smaller) one associated with the O atoms bridging two Gd atoms having moments of the same (opposite) signs. The sign of these O moments is opposite to that of the Gd moment with the larger magnitude. A three-dimensional plot of the spin density for $Gd_{12}O_{18}$ in the AFM state is shown in Figure 3. We can see that a significant spin polarization of charge density occurs only close to the Gd

TABLE 1: Electronic and Magnetic Properties of the Optimized $Gd_{12}O_{18}$ Cluster in the AFM and FM States from the Natural Population Analysis

	magnetic moment (μ_B)		natural electron configuration AFM (FM)	natural charge AFM (FM)
	AFM	FM		
Gd(A)	±7.02	7.02	$4f^{7.02}5d^{0.27}6s^{0.19}6p^{0.03}$	2.49
Gd(B)	±7.05	7.05	$4f^{7.02}5d^{0.43}6s^{0.18}6p^{0.05}$	2.32
O(a)	0.00	−0.02	$2s^{1.95}2p^{5.71}$	−1.66
O(b)	±0.01, ±0.02	−0.02	$2s^{1.96}2p^{5.63}$	−1.59
O(c)	±0.01, ±0.02	−0.02	$2s^{1.96}2p^{5.62}$	−1.58

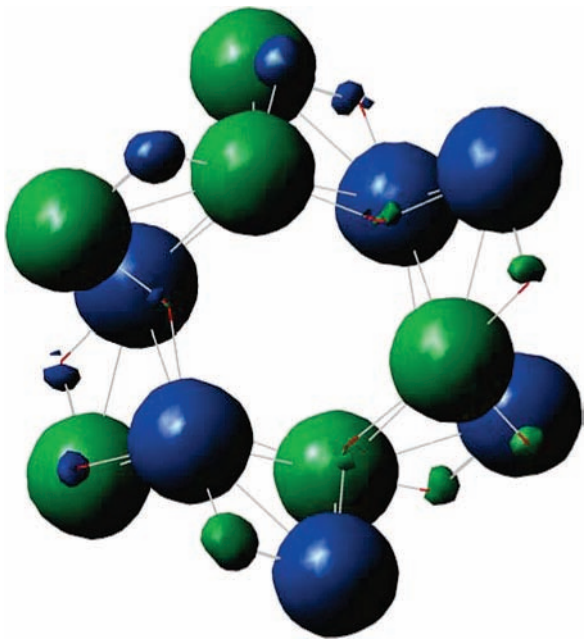

Figure 3. Three-dimensional plot of the spin polarization of the charge density for $Gd_{12}O_{18}$ in the AFM state; royal (olive) shades are positive (negative) isosurfaces for the value of ±0.005 electrons/au.

atoms. In the FM state the Gd magnetic moments have the same magnitude as in the AFM case, whereas the O moments are slightly larger in magnitude. The negative sign indicates that the induced magnetic moments on O atoms are coupled antiferromagnetically to the Gd moments. In both the AFM and FM cases, the magnitudes of the Gd moments are compatible with a spin of 7/2 that would result from Hund's rule for the half-filled 4f shell configuration, and thus a localized 4f spin moment picture can be envisaged.

The electron configurations for Gd and O atoms as derived from the natural population analysis are identical in both the AFM and FM states, and thus only the results for a single state are presented in Table 1. One can see that the occupation number (7.02 electrons) of Gd 4f orbitals is nearly equal to the number of the isolated $Gd^{3+}(4f^7)$, indicating the very little participation of the orbitals in bonding. The Gd 5d and 6s occupations in Table 1 indicate covalent Gd−O bonding contributions from these two types of orbitals, because the occupations substantially deviate from a purely ionic bonding between $Gd^{3+}(4f^7)$ and $O^{2-}(2s^22p^6)$ ions. The natural charges resulting from these electronic configurations are also reported in Table 1, from which it is seen that an average of 2.40 electrons per Gd atom is transferred to the O atoms. It should be noted that the occupation on the Gd 5d orbitals is attributed to a contribution of back-donation of the occupied O 2p orbitals. After this correction, the charge transfer from Gd to O is about 2.76 electrons.

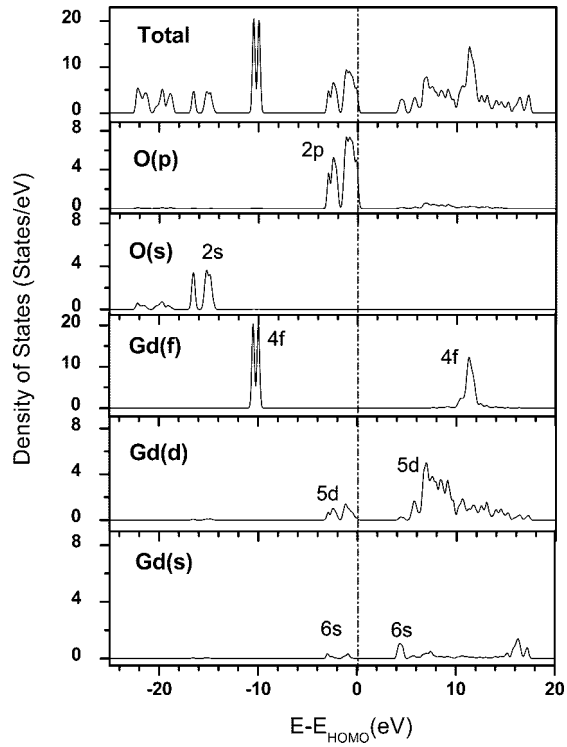

Figure 4. Total and orbital-projected partial DOS of $Gd_{12}O_{18}$ in the AFM state for one spin channel.

The total density of states (DOS) and the orbital-projected partial DOS (PDOS) for $Gd_{12}O_{18}$ in the AFM state are shown in Figure 4. Because of the zero spin polarization of the cluster, the DOS for the majority and minority spin channels are identical. The analysis of Figure 4 shows that the DOS in the energy region just below the highest occupied molecular orbital (HOMO) level is mainly due to the O 2p orbitals with small contributions from the 5d and 6s orbitals of Gd. The DOS in the energy region above the lowest unoccupied molecular orbital (LUMO) level is governed by the bands of Gd 5d and 6s characters. The 4f band split into two sub-bands; one is occupied and the other is unoccupied. The occupied 4f-electron states form a band in a narrow energy range (around −10 eV) well below the HOMO level with a two-peak structure; the lower- and higher-energy peaks arise from the Gd atoms in sites A and B, respectively. The unoccupied 4f band lies well above the LUMO level and hybrids with the unoccupied 5d band, giving rise to a broadening of the band. In the AFM state, the HOMO−LUMO gaps for the two spin channels are identical and have a value of 4.19 eV. In the FM state, the gap for the majority spin is 4.03 eV, whereas for the minority spin, it is 4.52 eV. Since the $Gd_{12}O_{18}$ cluster is more like a molecule than like a nanocrystal due to its limited size, it is not expected to exhibit the quantum confinement effect, i.e., an enlarged band gap relative to that of bulk Gd_2O_3 crystal of 5.44 eV.[39]

IV. Conclusions

We have investigated the magnetic coupling in the $Gd_{12}O_{18}$ cluster on the basis of SDFT electronic structure calculations in the broken-symmetry approach. The geometry optimizations have been performed for both the AFM and FM states. It was found that the optimized structures in the two states are almost identical, indicating that the participation of 4f orbitals in the bonding is negligible. The calculated energy of the FM state is 71.5 cm^{-1} higher than that of the AFM state, which gives a

value of about 0.24 cm^{-1} for the magnitude of the magnetic coupling constant between adjacent Gd ($4f^7$) spins. This value is comparable to that estimated from experiments on the bulk Gd_2O_3 crystal. Besides for these two states, the relative energies and spin patterns for the other broken-symmetry states have also been calculated. To gain insight into the origin of magnetic coupling in the cluster certain characteristics of the AFM state have also been discussed.

Our calculations indicate clearly an energetic preference for the AFM coupling between adjacent $4f^7$ spins in the $Gd_{12}O_{18}$ cluster, in contrast to the recent results of Pedersen and Ojamäe.[12] It should be noted, however, that the magnitude of the calculated magnetic coupling constant exhibit dependence on the amount of the Fock exchange in the HF/DFT hybrid functionals.[40−43] The presently used B3LYP functional contains about 20% Fock exchange. Tuning this amount may change the magnitude of the constant, but the qualitative description of the magnetic coupling will remain (see the discussions in refs 17, 18, and 43). Moreover, since the broken-symmetry method neglects the spin symmetry requirement in the wave function of the noninteracting reference system employed in the Kohn−Sham self-consistent procedure, a spin-restricted ensemble-referenced Kohn−Sham (REKS) method has been proposed, which results in a proper description of open-shell states where the total spin quantum number (S and M_s) are well-defined.[44,45] However, recent work showed that, with the present functionals, the REKS method gives no better description than the broken-symmetry one for the magnetic interactions, although the deviation with respect to experiments is rather systematic.[43]

The present results may have important implications for potential applications of Gd_2O_3 nanoparticles as MRI contrast agents. The small magnitude of the magnetic coupling constant indicates that the ground and excited spin states are close in energy, and the spin reversal barrier can be easily compromised by their thermal population. At room temperature the excited spin states are thermally populated, and therefore, the nanoparticles display nonzero magnetic moments and appear paramagnetic.

Acknowledgment. This work was supported by the NSFC (Grant Nos. 10804001, 10674002, and 20773024), National 863 projects (Grant No. 2006AA09Z243-3), and Program for Innovative Research Team in Anhui Normal University of China. The financial support from Fondazione CARIPLO-n.Prot.0018524 is also acknowledged.

References and Notes

(1) Gordon, W. O.; Carter, J. A.; Tissue, B. M. *J. Lumin.* **2004**, *108*, 339.
(2) Liu, G. K. In *Spectroscopic Properties of Rare Earths in Optical Materials*; Liu, G. K., Jacquier, B., Eds.; Tsinghua University Press: Tsinghua, China, 2005; pp 1−94.
(3) Guo, H.; Dong, N.; Yin, M.; Zhang, W.; Lou, L.; Xia, S. *J. Phys. Chem. B* **2004**, *108*, 19205.
(4) Chen, X.; Ma, E.; Liu, G.; Yin, M. *J. Phys. Chem. C* **2007**, *111*, 9638.
(5) Chen, X.; Ma, E.; Liu, G. *J. Phys. Chem. C* **2007**, *111*, 10404.
(6) Caravan, P.; Ellison, J. J.; McMurry, T. J.; Lauffer, R. B. *Chem. Rev.* **1999**, *99*, 2293.
(7) Endres, P. J.; Paunesku, T.; Vogt, S.; Meade, T. J.; Woloschak, G. E. *J. Am. Chem. Soc.* **2007**, *129*, 15760.
(8) Kim, J. S.; Rieter, W. J.; Taylor, K. M. L.; An, H.; Lin, W.; Lin, W. *J. Am. Chem. Soc.* **2007**, *129*, 8962.
(9) Engström, M.; Klasson, A.; Pedrsen, H.; Vahlberg, C.; Kall, P. O.; Uvdal, K. *Magn. Reson. Mater. Phys.* **2006**, *19*, 180.
(10) Fortin, M. A.; Petoral, R. M. P., Jr.; Söderlind, F.; Klasson, A.; Engström, M.; Veres, T.; Käll, P.-O.; Uvdal, K. *Nanotechnology* **2007**, *18*, 395501.
(11) Bridot, J.-L.; Faure, A.-C.; Laurent, S.; Riviere, C.; Billotey, C.; Hiba, B.; Janier, M.; Josserand, V.; Coll, J.-L. *J. Am. Chem. Soc.* **2007**, *129*, 5076.
(12) Pedersen, H.; Ojamäe, L. *Nano Lett.* **2006**, *6*, 2004.
(13) Shen, T.; Weissleder, R.; Papisov, M., Jr.; Brady, T. J. *Magn. Reson. Med.* **1993**, *29*, 599.
(14) Moon, R. M.; Koehler, W. C. *Phys. Rev. B* **1975**, *11*, 1609.
(15) Sorensen, C. M. In *Magnetism Nanoscale Materials in Chemistry*; Klabunde, K. J., Ed; Wiley: Heidelberg, Germany, 2001; pp 169−221.
(16) Kurz, Ph.; Bihlmayer, G.; Blügel, S. *J. Phys.: Condens. Matter* **2002**, *14*, 6353.
(17) Illas, F.; Moreira, I. P. R.; Graaf, C.; Barone, V. *Theor. Chem. Acc.* **2000**, *104*, 265.
(18) Moreira, P. R.; Illas, F. *Phys. Chem. Chem. Phys.* **2006**, *8*, 1645.
(19) Heisenberg, W. *Z. Phys.* **1928**, *49*, 619.
(20) Dirac, P. A. M. *Proc. R. Soc. London, Ser. A* **1929**, *123*, 714.
(21) Van Vleck, J. H. *The Theory of Electric and Magnetic Susceptibilities*; Clarendon: Oxford, U.K., 1932.
(22) Noodleman, L. *J. Chem. Phys.* **1981**, *74*, 5737.
(23) Noodleman, L.; Case, D. A. *Adv. Inorg. Chem.* **1992**, *38*, 423.
(24) Noodleman, L.; Peng, C. Y.; Case, D. A.; Mouesca, L.-M. *Coord. Chem. Rev.* **1995**, *144*, 199.
(25) Roy, L. E.; Hughbanks, T. *J. Solid State Chem.* **2003**, *176*, 294.
(26) Roy, L. E.; Hughbanks, T. *J. Am. Chem. Soc.* **2006**, *128*, 568.
(27) Sweet, L. E.; Roy, L. E.; Meng, F.; Hughbanks, T. *J. Am. Chem. Soc.* **2006**, *128*, 10193.
(28) Dai, D.; Whangbo, M. H. *J. Chem. Phys.* **2003**, *118*, 29.
(29) Becke, D. *J. Chem. Phys.* **1993**, *98*, 5648.
(30) Lee, C.; Yang, W.; Parr, R. G. *Phys. Rev. B* **1988**, *37*, 785.
(31) Frisch, M. J.; Trucks, G. W.; Schlegel, H. B.; Scuseria, G. E.; Robb, M. A.; Cheeseman, J. R.; Montgomery, J. A., Jr.; Vreven, T.; Kudin, K. N.; Burant, J. C.; Millam, J. M.; Iyengar, S. S.; Tomasi, J. J.; Barone, V.; Mennucci, B.; Cossi, M.; Scalmani, G.; Rega, N.; Petersson, G. A.; Nakatsuji, H.; Hada, M.; Ehara, M.; Toyota, K.; Fukuda, R.; Hasegawa, J.; Ishida, M.; Nakajima, T.; Honda, Y.; Kitao, O.; Nakai, H.; Klene, M.; Li, X.; Knox, J. E.; Hratchian, H. P.; Cross, J. B.; Adamo, C.; Jaramillo, J.; Gomperts, R.; Stratmann, R. E.; Yazyev, O.; Austin, A. J.; Cammi, R.; Pomelli, C.; Ochterski, J. W.; Ayala, P. Y.; Morokuma, K.; Voth, A.; Salvador, P.; Dannenberg, J. J.; Zakrzewski, V. G.; Dapprich, S.; Daniels, A. D.; Strain, M. C.; Farkas, O.; Malick, D. K.; Rabuck, A. D.; Raghavachari, K.; Foresman, J. B.; Ortiz, J. V.; Cui, Q.; Baboul, A. G.; Clifford, S.; Cioslowski, J.; Stefanov, B. B.; Liu, G.; Liashenko, A.; Piskorz, P.; Komaromi, I.; Martin, R. L.; Fox, D. J.; Keith, T.; Al-Laham, M. A.; Peng, C. Y.; Nanayakkara, A.; Challacombe, M.; Gill, P. M. W.; Johnson, B.; Chen, W.; Wong, M. W.; Gonzalez, C.; Pople, J. A. Gaussian03, revision B.05; Gaussian, Inc.: Pittsburgh, PA, 2003.
(32) Martin, R. L. *Electronic Structure: Basic Theory and Practical Methods*; Cambridge University Press: Cambridge, U.K., 2004; pp 152−171.
(33) Maron, L.; Eisenstein, O. *J. Phys. Chem. A* **2000**, *104*, 7140.
(34) Hay, P. J.; Martin, R. L.; Uddin, J.; Scuseria, G. E. *J. Chem. Phys.* **2006**, *125*, 034712.
(35) Clark, E. *J. Chem. Theory Comput.* **2008**, *4*, 708.
(36) Pedersen, H.; Söderlind, F.; Petoral, R. M.; Uvdal, K.; Käll, P.-O.; Ojamäe, L. *Surf. Sci.* **2005**, *592*, 124.
(37) Cundari, T. R.; Stevens, W. J. *J. Chem. Phys.* **1993**, *98*, 5555.
(38) Reed, A. E.; Weinstock, R. B.; Weinhold, F. *J. Chem. Phys.* **1985**, *83*, 735.
(39) Mercier, B.; Ledoux, G.; Dujardin, C.; Nicolas, D.; Masenelli, B.; Mélinon, P.; Bergeret, G. *J. Chem. Phys.* **2007**, *126*, 044507.
(40) Martin, R. L.; Illas, F. *Phys. Rev. Lett.* **1997**, *79*, 1539.
(41) Illas, F.; Martin, R. L. *J. Chem. Phys.* **1998**, *108*, 2519.
(42) Ciofini, I.; Illas, F.; Adamo, C. *J. Chem. Phys.* **2004**, *120*, 3811.
(43) Moreira, P. R.; Costa, R.; Filatov, M.; Illas, F. *J. Chem. Theory Comput.* **2007**, *3*, 764.
(44) Filatov, M.; Shaik, S. *Chem. Phys. Lett.* **1998**, *288*, 689.
(45) Filatov, M.; Shaik, S. *Chem. Phys. Lett.* **1999**, *304*, 429.

JP807015B